Journal of Applied Polymer Science

Toughening of syndiotactic polypropylene with chalk

Lukasz Pietrzak, Przemyslaw Sowinski, Joanna Bojda, Ewa Piorkowska, Andrzej Galeski
Centre of Molecular and Macromolecular Studies, Polish Academy of Sciences, Sienkiewicza 112, Lodz 90 363, Poland
Correspondence to: E. Piorkowska (E-mail: epiorkow@cbmm.lodz.pl)

ABSTRACT: We hypothesized that polymer crystal anisotropy is advantageous for toughening of polymer composites involving easy slip network of oriented crystalline layers around filler particles. To this end, composites of syndiotactic polypropylene (sPP) with high concentration of submicrometer calcium carbonate particles were prepared and examined because usual sPP crystals exhibit high packing anisotropy. The specific orientation of sPP lamellae around chalk grains was found, which is supposed to facilitate the plastic deformation of polymer matrices. The compression molded bars of the composite exhibited markedly higher Izod impact strength than those of neat sPP. Toughening was even enhanced in the injection molded composite, for which 4.5-fold increase in the impact strength was achieved. Injection-induced orientation of the disordered form I sPP crystals was enhanced in the composite. The injection molded tensile specimens exhibited also a good drawability. Debonding at chalk–sPP interface occurred both during the impact and tensile tests facilitating the plastic deformation of sPP matrix. Chalk did not have any significant influence on the thermal properties of the composites but it affected the rheological behavior, increasing the loss and storage moduli, and the viscosity. Highly filled sPP composite exhibited solid-like behavior in a molten state with the storage modulus exceeding the loss modulus in the entire frequency range. © 2016 Wiley Periodicals, Inc. J. Appl. Polym. Sci. **2016**, *133*, 43651.

KEYWORDS: composites; mechanical properties; polyolefins

Received 12 January 2016; accepted 18 March 2016
DOI: 10.1002/app.43651

INTRODUCTION

Polymer composites are long known and used as they offer many advantages in comparison to neat polymers. In systems with rigid fillers, only a polymer matrix is tough and able to undergo plastic deformation. The concentration of stress causes a build-up of triaxial stresses around filler particles, which leads to debonding at the particle–matrix interface. The voids alter the stress-state of the polymer matrix which facilitates shear yielding. Chalk–calcium carbonate is frequently applied as a filler because of high chemical purity, high degree of whiteness, low abrasiveness, good dispersibility, and approval for food contact. Bartczak *et al.*[1–3] investigated the mechanical properties of high-density polyethylene (HDPE) filled with different grades of calcium stearate-treated chalk with particles having average size (by weight) of 3.50, 0.70, and 0.44 μm in various fractions ranging up to 30 vol %, that is, 55 wt %, and reported dramatic 12-fold increase of toughness when the mean interparticle ligament thickness of the matrix decreased below 0.6 μm. The studies of HDPE crystallized adjacent to (104) crystallographic planes of calcite demonstrated that lamellar HDPE crystallites preferentially grew "edge-on" on calcite.[4] Therefore, it was assumed that in the composites, chalk particles were enveloped by 0.3–0.4-μm-thick shells of specifically oriented HDPE crystallites. It was postulated further that the source of toughness was crystal plasticity in those oriented layers percolated throughout the material. When the average ligament thickness is less than the critical value, a dramatic jump of toughness results. The usual strength-limiting microstructural flaws become ineffective and superior toughness at impact strain rates is achieved. The important point is that only modest adhesion between the rigid particles and matrix is advantageous because of the need of debonding (the cavitation at interfaces) that is necessary to facilitate the plastic deformation of the surrounding polymer. Moreover, the same mechanism was proposed to explain increased toughness of HDPE and polyamide blends with rubber.[3,5–7] In blends, the dispersed rubber has either to cavitate or to debond from the surrounding matrix phase.

However, others[8–11] indicated the flow-induced crystal orientation as a possible reason for existence of a critical interparticle ligament thickness for toughening semicrystalline polymers composites and blends. Numerical simulation[11] demonstrated that the presence of rigid particles in sheared polymer melts resulted in inhomogeneous stretch of macromolecules, that is, high molecular stretch in regions between two particles and near the top and the bottom of neighboring particles, and also regions with a molecular stretch lower than in neat polymer melt for the same flow.

Galeski and Bartczak[12] pointed out that the unusual toughening was observed for polyamides and polyethylene; that is, for the polymers which crystals show high anisotropy for plastic deformation; the easiest slip of orthorhombic polyethylene crystals occurs at 7.2 MPa, that is, at shear stress much lower than 12.2 and 15.6 MPa required for the other slips.[13] The α crystals of polyamide 6 also exhibit anisotropy with shear stresses for crystallographic slips 16.2, 23.0, and 23.2 MPa.[14] One can conclude that the packing anisotropy is advantageous for polymer crystals to form the easy slip network. The differences in the critical shear stresses required for the slips are low for monoclinic crystals of isotactic polypropylene and for crystals of polyoxymethylene described as hexagonal or trigonal. We note that toughening of isotactic polypropylene was achieved by incorporation of submicron[15] or nanosized chalk particles, but in the latter only after surface treatment improving adhesion.[16–18] Levita *et al.*[18] analyzed the fracture energy in terms of the crack pinning model but due to the very small size of particles the pinning contribution proved to be negligible.

In general, the source of differences in the critical shear stresses for plastic deformation is packing density in the respective crystallographic planes; the slips occur easily along the planes of the most dense packing. Our study was aimed at proving the hypothesis that the crystal anisotropy is advantageous for the toughening mechanism acting in polymer composites, where the source of toughness is the crystal plasticity in oriented layers formed around filler particles percolated through the material. To this end, composites of syndiotactic polypropylene (sPP) crystallized in the disordered form I with 5–17 vol % of chalk modified with calcium stearate, having average grain size of 0.85 μm, were prepared and examined.

According to De Rosa *et al.*[19] and De Rosa and Auriemma,[20] the most stable orthorhombic limit-ordered form I of sPP can be obtained from melt only when the highly stereoregular polymer crystallizes at high temperatures. Otherwise, the disordered form I and the form II crystallize from melt, with orthorhombic and C-centered orthorhombic anisotropic unit cells, respectively, having axes: $a = 1.45$ nm, $b = 0.56$ nm, and $c = 0.74$ nm.

Possibility to toughen syndiotactic polypropylene (sPP) by filling with chalk was shown by Galeski and Bartczak.[12] However, Supaphol *et al.*[21] studied the effect of chalk particle size (from 1.9 to 10.5 μm), content (up to 40 wt %), and the type of surface modification on the thermal and mechanical properties of sPP composites and concluded that the impact resistance decreased with increasing particle content and size. Only sPP with low contents of 1.9 μm chalk particles exhibited the impact strength slightly higher than that of neat sPP. Also the tensile strength of the composites decreased with increasing filler content. However, the effect of further decrease of a particle size was not explored, and possibly the interparticle ligament thickness was not decreased below its critical value.

In this contribution, submicrometer chalk particles were used and both compression molding and injection molding were employed for sample preparation to evaluate the effect of formation of easy slip network of oriented crystalline layers around filler particles. The structure as well as the tensile, impact, rheological, and thermal properties of the composites were studied.

EXPERIMENTAL

The study utilized sPP provided by Sigma Aldrich (St. Louis, MO) having molar mass M_w of 174 kg mol^{-1}, $M_w M_n^{-1}$ of 2.3, syndiotacticity of 93%, and melt flow index of 2.2 g (10 min)$^{-1}$ (230 °C, 2.16 kg). Ground chalk (calcite) Hydrocarb 95T, with the weight average particle size of 0.85 μm, modified with 2–2.8 wt % of calcium stearate, was provided by Omya.

The composites with 5, 10, and 17 vol % of the filler (dried in vacuum oven at 120 °C for 12 h) were prepared by mixing the components at 60 rpm for 10 min at 180 °C in a Brabender batch mixer (Duisburg, Germany). The volume contents correspond to 13, 24, and 37 wt %, respectively. The composites will be referred to as for example sPP/CC-5, where the number stands for a filler volume content. Neat sPP was processed in the same way to obtain a reference material.

To examine mechanical properties, compression molded and injection molded samples were prepared. Plates of 4 mm thickness were compression molded at 180 °C for 5 min and then quenched in ice water. For the Izod impact tests, bars with shapes conforming to ISO 180 standard were cut from the plates. Five grams laboratory injection molding machine (PROMA, Poland) was used at the injection molding temperature of 180 °C, pressure of 0.65 MPa, and the form temperature of 50 °C to inject 4-mm-thick bars with the other sizes conforming to ISO 180 standard and 2-mm-thick oar-shaped tensile specimens with 20 and 4 mm gauge length and width, respectively.

Prior to impact testing, 0.5 mm skin layer was removed from all the bars using a milling machine to produce flat and parallel surfaces. Next, the bars were notched according to ISO 180 and allowed to relax for at least 24 h. Notched Izod impact tests were performed at room temperature (RT) on at least 5 specimens of each material by means of an impact hammer RESIL5.5, CEAST (Charlotte,NC) having maximum energy of 5.5 J and velocity of 3.5 m s^{-1}.

Tensile tests were carried out on an Instron 5582 machine (High Wycombe, UK) at RT at the strain rate of 50% min^{-1}, on at least 3 specimens of each material.

Fracture surfaces of the samples were sputtered with gold and studied under a scanning electron microscope (SEM) JEOL JSM-LV5500 (Tokyo, Japan).

Atomic force microscope (AFM) Nanoscope IIIa (Veeco, NY) running in a tapping mode was used for analysis of lamellar structure of sPP in 0.5-mm-thick films crystallized with free upper surfaces in Mettler Toledo FP82H hot stage (Greifensee, Switzerland). The films were heated to 200 °C, melt annealed for 3 min, cooled at 20 °C min^{-1} to 80 °C, isothermally crystallized for 1 h and quenched to RT, according to the protocol based on preliminary studies.

The crystal structure was probed with a wide-angle X-ray scattering (WAXS) system, with a computer-controlled wide-angle goniometer coupled to a sealed-tube source of CuK$_\alpha$ radiation

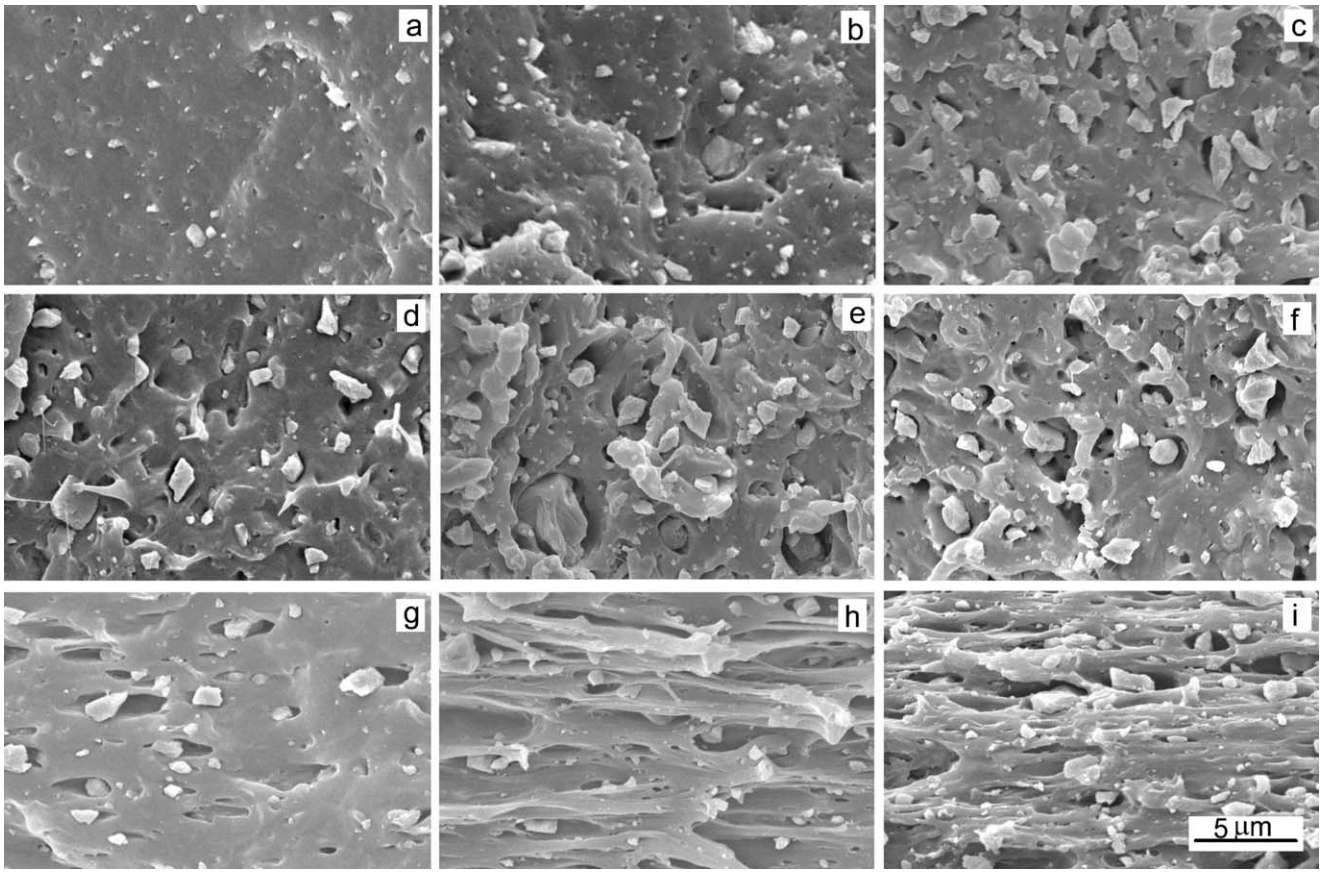

Figure 1. SEM micrographs of sPP/CC composites: (a) surfaces of cryo-fractured sPP/CC-5, (b) sPP/CC-10, and (c) sPP/CC-17, fracture surfaces of impacted specimens: (d) sPP/CC-10 injected, (e) sPP/CC-17 injected, and (f) sPP/CC-17 compression molded, injection molded tensile specimens drawn until fracture and then cryofractured along a plane parallel to the drawing direction (horizontal): (g) sPP/CC-5, (h) sPP/CC-10, and (i) sPP/CC-17. The scale bar in (i) applies to all micrographs in Figure 1.

(Philips, Eindhoven, The Netherlands), operating at 30 kV and 50 mA. The CuK_α line was filtered using electronic filtering and the usual thin Ni filter. The slit system that was used for collecting 2θ scans allowed for the collection of the diffracted beam with the divergence angle of $<0.05°$. Determination of the sPP crystal orientation was performed with a WAXS camera coupled to X-ray generator (sealed-tube, fine point CuK_α filtered source operating at 30 kV and 30 mA, Philips) using Pilatus 2D detector.

The oscillatory rheological measurements were carried out in rheometer ARES LS2 TA Instruments, in a cone-plate geometry (25 mm diameter, 0.1 rad cone angle, 0.05 mm gap) in the temperature range from 170 to 220 °C. Disks of 1 mm thickness with the diameter of 25 mm, compression molded at 190 °C, were placed in the measuring cell and heated to 220 °C. Next, the gap was set and temperature was either kept constant or decreased to a desired level. Low-amplitude oscillatory shear experiments were carried out within the linear viscoelastic regime over the frequency (ω) range of 0.1–512 rad s^{-1} beginning with the highest ω. The linear regimes of viscoelasticity were determined during preliminary strain sweep tests.

Thermal properties were investigated during heating at 10 °C min^{-1} to 200 °C under a flow of nitrogen using differential scanning calorimeter DSC 2920 (TA Instruments, New Castle, DE). To study crystallization, the specimens were quickly heated to 200 °C, melt annealed for 3 min, and cooled to RT at 10 °C min^{-1}.

RESULTS AND DISCUSSION

Exemplary SEM micrographs of the composites are shown in Figure 1. Majority of chalk is seen in the form of well-dispersed single particles, with only occasional aggregates.

Figure 2, which compares the rheological properties of the materials, evidences that decreasing temperature enlarged the storage (G') and loss (G'') modulus, and the complex viscosity (η^*), the latter decreased with increasing ω due to shear thinning. All three—G', G'', and η^*—increased with increasing chalk content. Such behavior is typical of polymer composites including sPP filled with chalk.[22] However, in the case of sPP/CC-17, a decrease of temperature to 170 °C resulted in a change to a solid-like behavior, with G' exceeding G'' in the entire ω range. Moreover, at 170 °C in the low ω range, the η^* of sPP/CC-17 was two orders of magnitude larger than that of sPP/CC-10. The solid-like behavior of sPP/CC-17 arose from the formation of a network structure, absent at lower filler contents, and reflected strong interparticle interactions due to decreased interparticle distances in the composite.

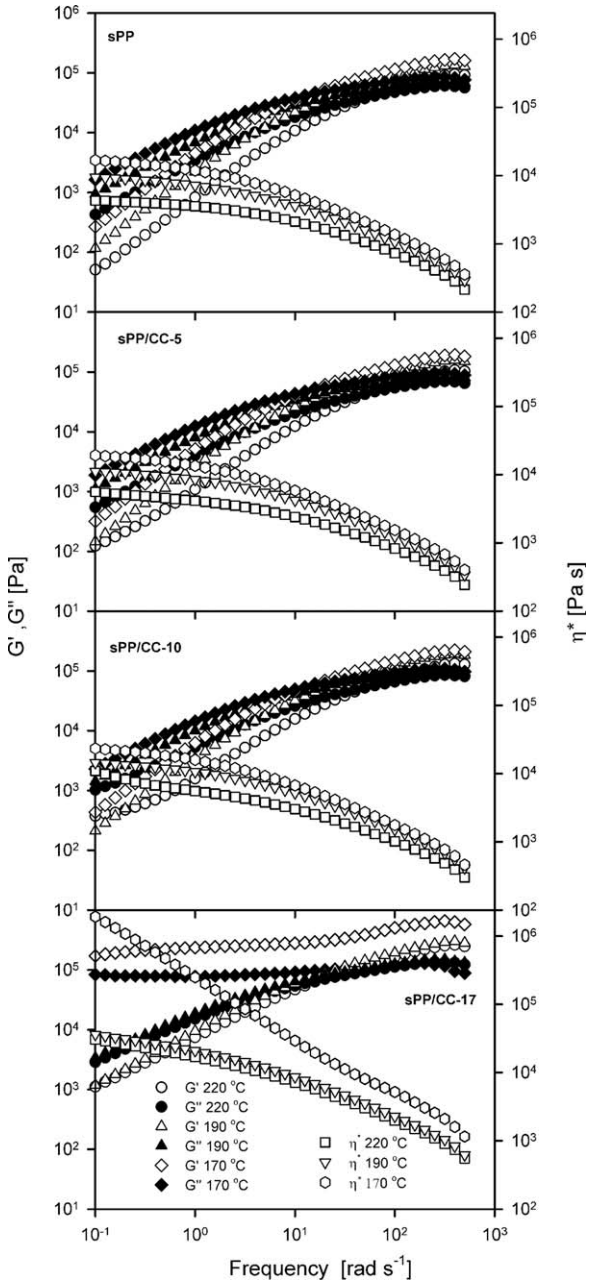

Figure 2. Rheological properties of neat sPP and sPP/CC composites.

Figure 3 shows that during cooling in DSC, the presence of chalk weakly affected the peak crystallization temperature of sPP in the composites, which was about 81–82 °C for all the materials. Such lack of changes in crystallization temperature during cooling was already reported by Supaphol *et al.*[21] for sPP filled with either stearic acid- or paraffin-coated chalk. The melting behavior of the materials during subsequent heating was also similar, with double peak melting endotherms, at 119 and 129 °C. The peak at higher temperature can result from melting of the crystals recrystallized during a heating scan[23]; sPP crystallized at relatively high temperature exhibits a single high-temperature melting peak. The melting enthalpy was about 40 J g_{sPP}^{-1} for all the materials which corresponds to the crystallinity level of 21 wt % if heat of fusion of crystals equal to 190.5 J g^{-1} is assumed.[24]

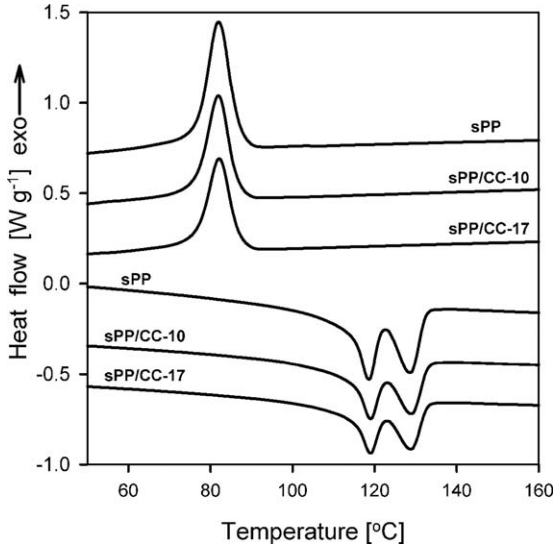

Figure 3. DSC cooling and subsequent heating thermograms of neat sPP and sPP/CC composites. Curves are shifted vertically for better visualization.

The Izod impact strength, *U*, of the composites is shown in Figure 4. Only sPP/CC-5 and sPP—both compression and injection molded—broke completely during the impact test, while sPP/CC-10 and sPP/CC-17 broke only partially. *U* of sPP/CC-5 did not exceed that of neat sPP. Contrary to that, *U* of sPP/CC-10 and especially of sPP/CC-17 was improved; *U* of the compression molded sPP/CC-17 was 2.2 times higher than that of the compression molded neat sPP. Up to 10 vol % chalk content *U* of the injection and compression molded materials was similar within the limits of experimental errors. However, injection molding of sPP/CC-17 led to 1.5-fold increase of *U* compared to the compression molded composite.

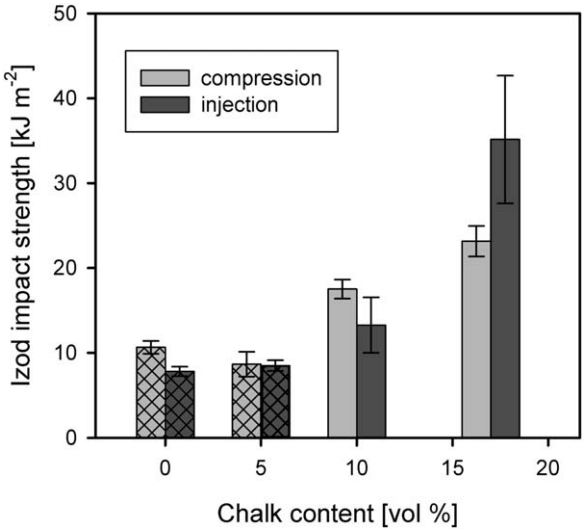

Figure 4. The Izod impact strength of sPP and sPP composites; squared pattern indicates samples, which completely broke during impact: sPP and sPP/CC-5.

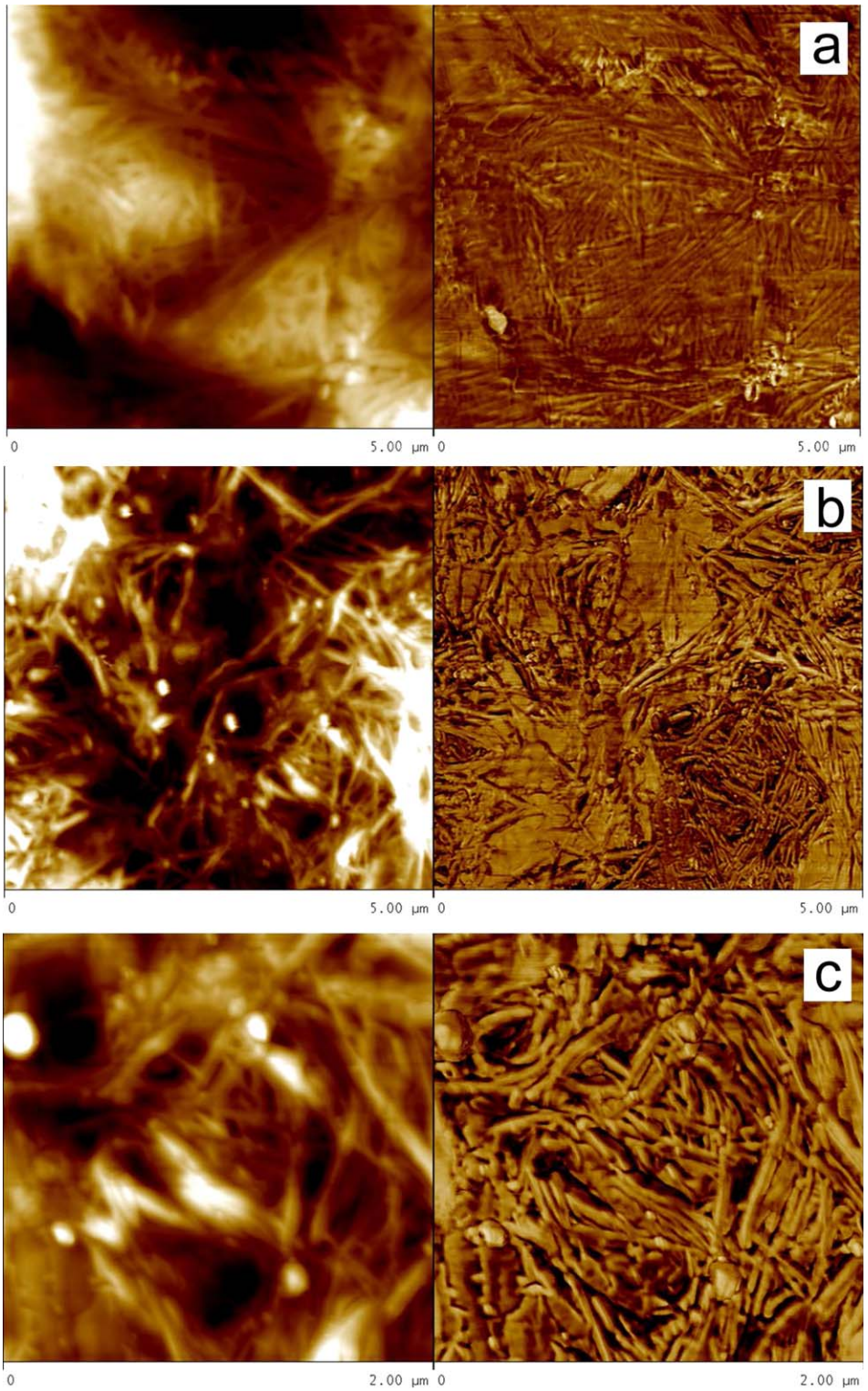

Figure 5. AFM images of isothermally crystallized (a) sPP and (b,c) sPP/CC-17. [Color figure can be viewed in the online issue, which is available at wileyonlinelibrary.com.]

Toughening of polymers with rigid particulate fillers is well recognized; the concentration of applied stress around filler particles causes debonding at the filler–matrix interface, which further facilitates shear yielding of the liberated matter, e.g., refs. 15,25,26. Indeed, SEM analysis of fracture surfaces of the composites evidenced separation of the chalk grains from sPP matrix during the impact test, as it is exemplified in Figure 1(d–f), showing both injection molded and compression

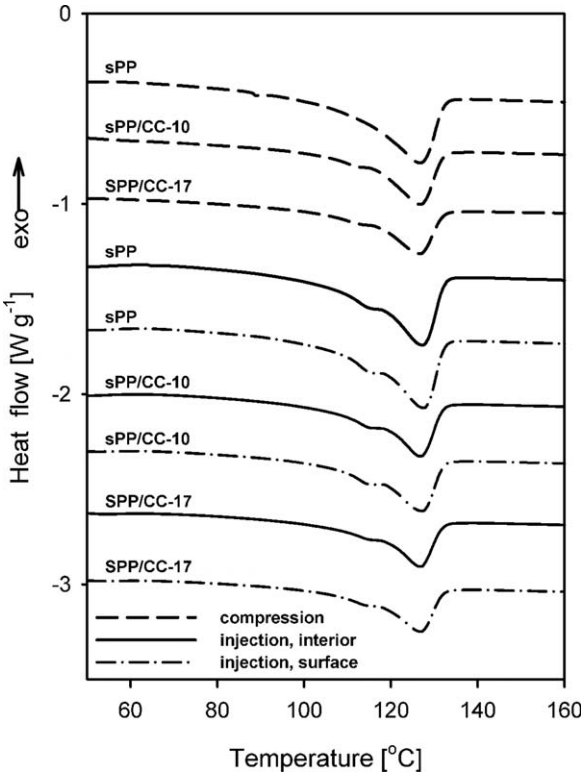

Figure 6. DSC heating thermograms of specimens of impacted bars of sPP and sPP/CC composites, both compression and injection molded. Curves are shifted vertically for better visualization.

molded sPP/CC-17. As already mentioned above, the separation of a filler from a matrix is required for easy plastic deformation of the latter. However, according to Bartczak *et al.*,[4,5] the sources of toughness are both debonding and crystal plasticity in specifically oriented lamellae surrounding filler particles and percolating through the matrix.

Indeed, despite similar crystallization and melting behavior, the lamellar structure of the composites differs from that of neat sPP as it is evidenced by the AFM images in Figure 5. In neat sPP lamellae radiate from a common center, typically of spherulitic structure. In sPP/CC-17 chalk grains, with sizes between 1 and 2 μm, are surrounded by edge-on positioned lamellae, and, additionally, packs of lamellae extend from one grain to another. Interestingly, such orientation of lamellae, edge-on with respect to filler grains, can be seen even around small particles, with size well below 1 μm, as it is shown in Figure 5(c). Such lamellae orientation with respect to foreign surfaces was frequently reported for thin polymer films, including nanolayers of polyolefins.[27–29] In sPP nanolayers (the same grade as used in our study), sandwiched between polycarbonate layers, increasing tendency to form edge-on lamellae with decreasing crystallization temperature was found[29]; in 120-nm-thin layers exclusively edge-on lamellae formed below 90 °C. Prevailing edge-on lamellae orientation is attributed to nucleation of crystals induced by the parallel alignment of coil segments of molten polymer in contact with the hard walls.[30]

During injection molding, not only cooling but also a flow influences crystallization and resulting polymer morphology. The structure of injection molded bars was studied by DSC and WAXS, and compared to that of their compression molded counterparts. Figure 6 presents the exemplary DSC heating thermograms of the specimens cut out from both surface and interior layers of the bars. In the case of injection molded bars, the specimens were cut out from the central and side zones of the both layers. The melting behavior of specimens from different zones of the bars was similar; hence, only exemplary thermograms are plotted in Figure 6. All the thermograms are featured by melting peaks centered about 126–127 °C. Except for the compression molded sPP, the melting peaks of the materials exhibited shoulders at 114–115 °C. The melting enthalpy was similar in all cases, 35–38 J g_{sPP}^{-1} for both compression and injection molded bars. The differences in melting behavior of specimens cut out from the bars and those crystallized in DSC, presented in Figure 3, resulted undoubtedly from different cooling conditions, and also from a possible effect of flow during injection. It must be mentioned that the presence of chalk increases thermal conductivity of the material, thus improving subtraction of heat during cooling.

Figure 7 compares the WAXS curves of specimens of compression and injection molded bars, after removing the skin layer similarly as for the impact test, studied in a transmission mode; the curves were corrected for absorption caused predominantly by calcium in chalk grains according to ref. 31. For examination, 1-mm-thick specimens were cut out from a zone equally distant from the bar ends, from the surface layer, as on the scheme in the upper right corner of Figure 7, depicting a position of the specimen on the cross-section of the bar and the X-ray incident beam direction. The WAXS curves evidence sPP disordered form I, as can be

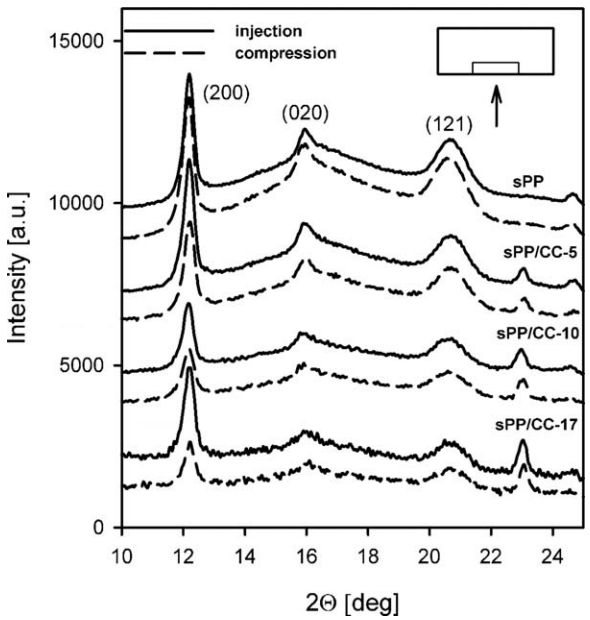

Figure 7. WAXS diffractograms of impacted bars of sPP and sPP/CC composites injected and compression molded. Curves are corrected for X-ray absorption and shifted vertically for better visualization. Location of the specimens cut from the bars shown in the upper right corner.

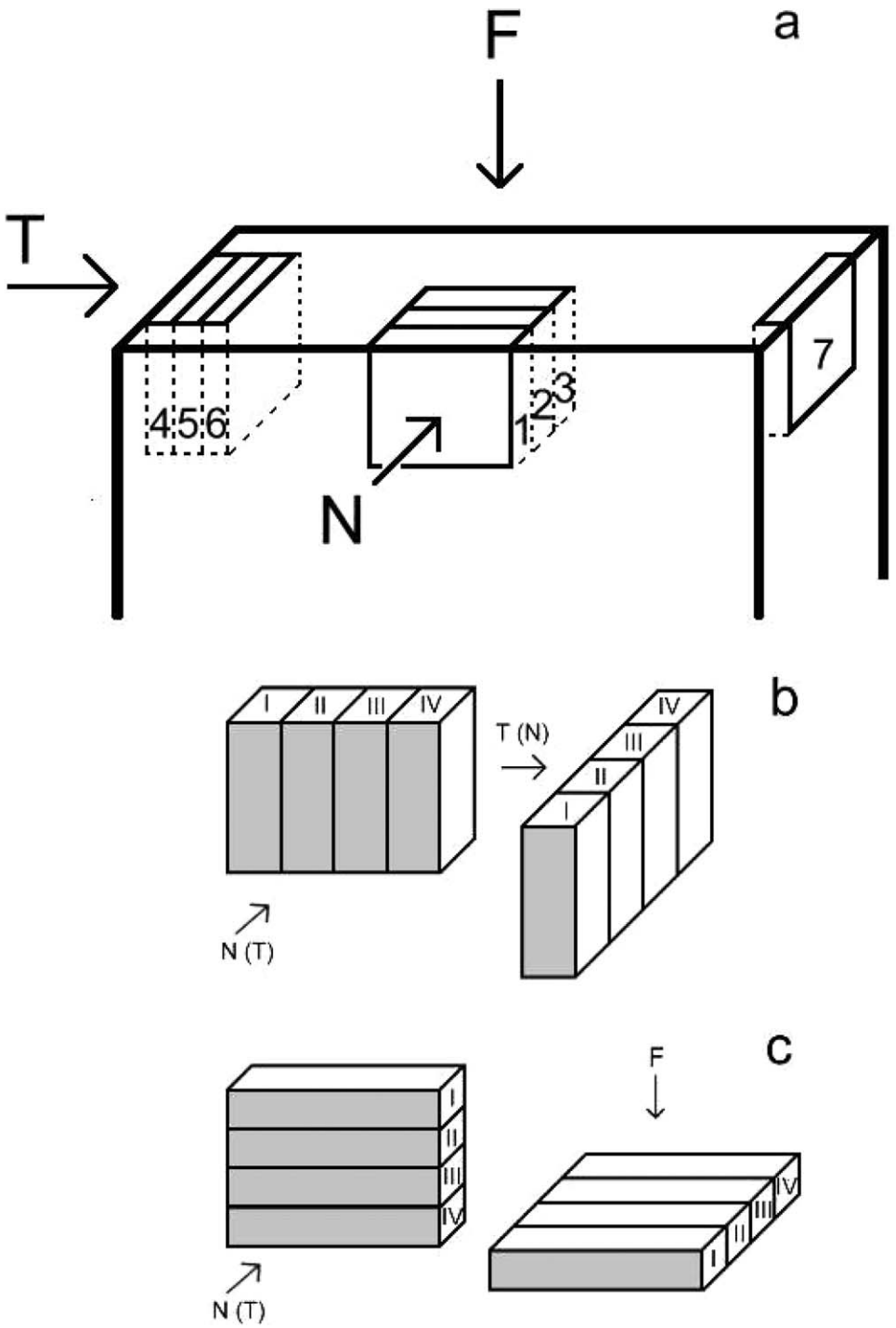

Figure 8. Scheme of (a) cutting specimens from impact bars and (b,c) cutting and rearranging of the specimens for illumination with X-ray beam in the other directions.

judged from the presence of (200), (020), and (121) reflections at predicted 2θ positions[20] and the absence of (211) reflection at $2\theta = 18.8°$ characteristic of the limit-ordered form I.[32] All the curves exhibit strong (200) reflection at $2\theta = 12.2°$. It can be seen that the difference between compression and injection bars in magnitude of (200) reflection increased with chalk content. This clearly indicates orientation of sPP crystals in the injection molded bars, which was further corroborated by 2D-WAXS.

For 2D-WAXS examination, ~0.7-mm-thick specimens were cut out from the injection bars of sPP and sPP/CC-17 in the middle of bar length, as shown in Figure 8(a). The as-cut specimens 1, 2, and 3 were illuminated with the incident X-ray beam in the normal direction (ND). After examination, the specimens were cut into vertical strips, which were rearranged and illuminated in the transversal direction (TD) [Figure 8(b)]. The as-cut specimens 4, 5, and 6 were first exposed to the beam in the TD,

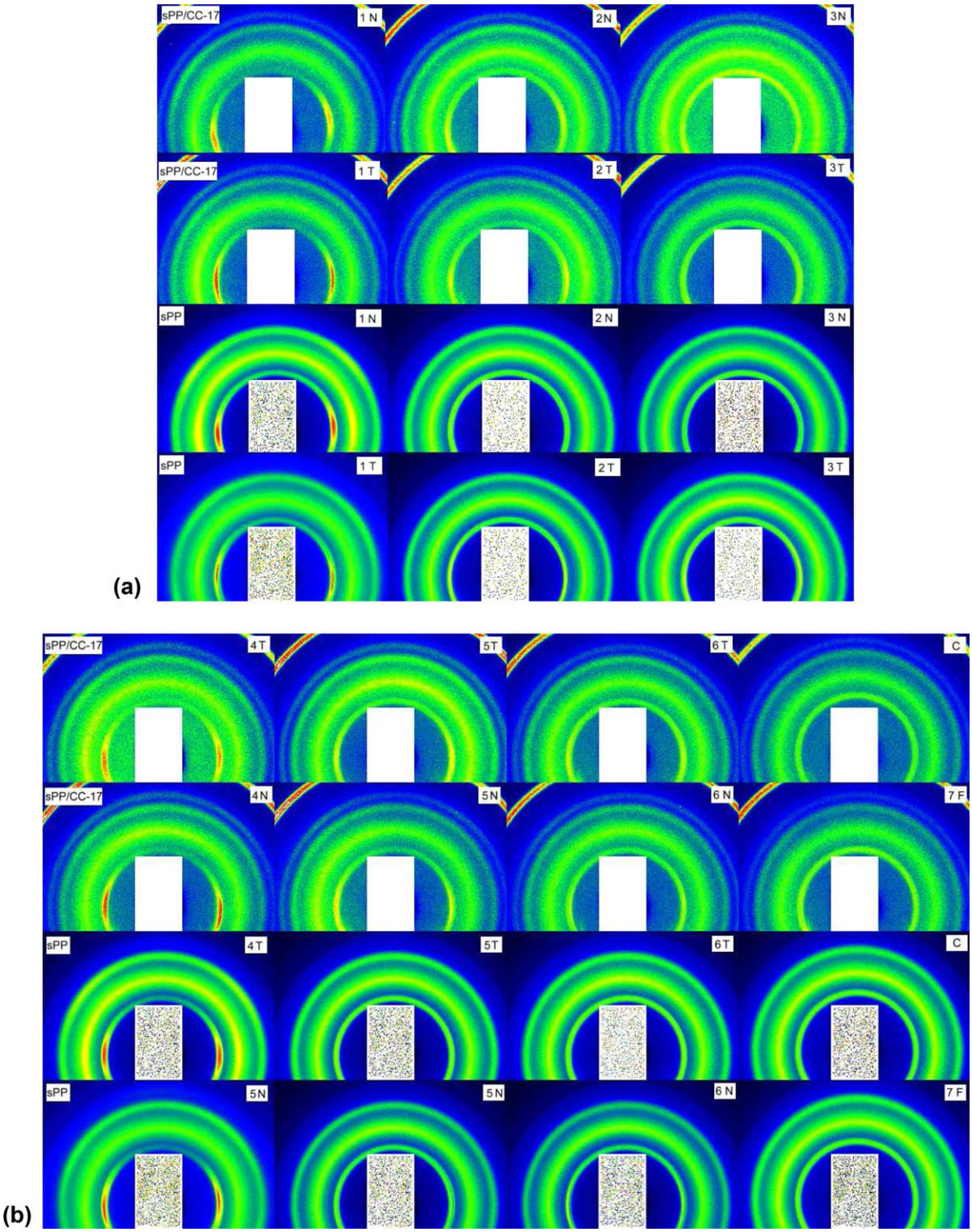

Figure 9. (a) 2D-WAXS patterns of injected bars sPP and sPP/CC-17 specimens 1, 2, and 3 for X-ray incident beam in N and T directions. (b) 2D-WAXS patterns of injected bars sPP and sPP/CC-17 specimens 4, 5, and 6 for X-ray incident beam in T and N directions, specimens 7 illuminated in F direction, and exemplary 2D-WAXS patterns of compression molded bars labeled as C, for comparison. [Color figure can be viewed in the online issue, which is available at wileyonlinelibrary.com.]

and after rearrangement, in the ND. The specimens 7 were cut in horizontal strips, which were arranged vertically and 2D-WAXS patterns were recorded with the incident beam in the flow direction (FD), as shown in Figure 8(c). Some specimens cut out from other zones of the bars were also illuminated in the FD. The recorded 2D-WAXS patterns are collected in Figure 9(a,b). It appears that sPP/CC-17 specimen 1, illuminated in both ND and TD, shows strong equatorial (200) reflections

evidencing orientation of crystals with (200) planes parallel to the FD. The orientation was weaker in the specimen 2 and only very weak in the specimen 3 from the core of the bar. The patterns of sPP specimen 1, illuminated in both ND and TD, also show strong equatorial (200) reflections evidencing orientation of crystals with (200) planes parallel to the FD but only very weak orientation is reflected on the patterns of specimens 2 and 3 illuminated in the TD and none for illumination in the ND. The difference between crystal orientation in sPP and sPP/CC-17 is even better visible on the patterns of the specimens 4, 5, and 6. The strong equatorial (200) reflections are seen on the patterns of sPP/CC-17 specimens illuminated in both TD and ND. Although their intensity decreased for specimens 5 and 6, still the respective patterns evidence the orientation, although weaker. Contrary to that, only the patterns of sPP specimen 4 exhibit the crystal orientation, whereas those of specimens 5 and 6 do not. The 2D-WAXS patterns of sPP and sPP/CC-17 specimens 7 and any other illuminated in the FD did not evidence any crystal orientation, indicating that the orientation, stronger in the composite and weaker in neat sPP, is only in respect to the FD. It must be noted that on the patterns evidencing strong orientation of (200) planes parallel to the FD also an enhancement of equatorial (020) reflection intensity is seen, showing orientation of (020) planes parallel to the FD. As expected, the 2D-WAXD patterns of specimens cut from compression molded bars evidenced crystal orientation neither in sPP nor in sPP/CC-17, regardless of specimen position in the bars and illumination direction.

Exemplary stress–strain curves for the injection molded tensile specimens are plotted in Figure 10, whereas the mechanical properties are summarized in Table I. In general, the presence of chalk particles decreased the yield stress (σ_y) and strain whereas the stress (σ_b) and strain at break (ε_b) slightly increased. The decrease of σ_y evidenced that the filler particles facilitated the plastic deformation of the matrix. SEM micrographs of the specimens, drawn to fracture and next cryo-fractured in a plane parallel to the drawing direction, shown in Figure 1(g–i), clearly evidence cavities around chalk particles, elongated in the drawing direction. Earlier yielding of the composite indicates that the debonding occurred prior to yield of the matrix, which is a prerequisite for toughening.

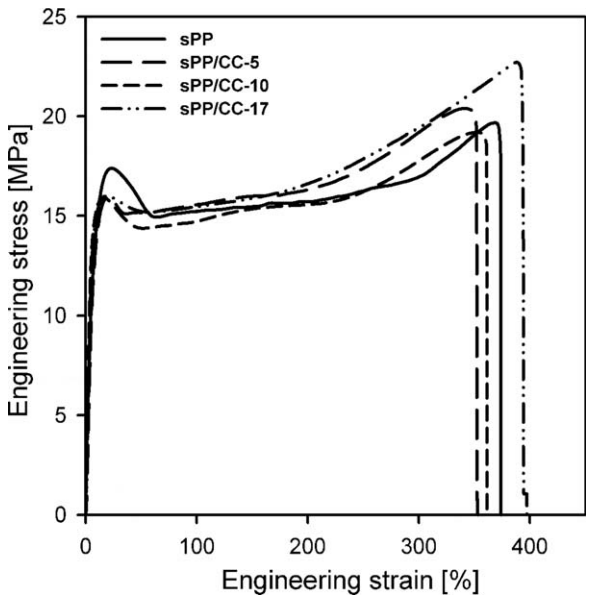

Figure 10. Stress–strain dependencies of injection-molded sPP and sPP/CC composites.

Table I. Average Values and Standard Deviations (in Brackets) of Mechanical Parameters of Neat sPP and sPP/CC Composites: Yield Stress (σ_y), Stress (σ_b), and Strain at Break (ε_b)

Sample code	σ_y [MPa]	σ_b [MPa]	ε_b [%]
sPP	16.1 (1.3)	19.9 (1.9)	381 (23)
sPP/CC-5	15.8 (0.3)	20.6 (0.7)	398 (27)
sPP/CC-10	15.7 (0.5)	20.5 (1.5)	397 (14)
sPP/CC-17	14.6 (0.7)	21.0 (2.3)	401 (19)

CONCLUSIONS

Composites of sPP with chalk having submicrometer average grain size were prepared and studied. Filling sPP with chalk did not affect markedly its thermal properties. In contrast, the rheological properties were strongly influenced; G', G'', and η^* increased with increasing chalk content. The effect of chalk was the strongest in sPP/CC-17 composite; at 170 °C, this composite exhibited a solid-like behavior with G' exceeding G'' in the entire ω range from 0.1 to 512 rad s^{-1}. Evidently, a network structure and strong interparticle interactions due to decreased interparticle distances is formed in the composite with high filler content. Such network is absent at lower filler content.

The incorporation of 17 vol % of chalk with 0.85 μm grain size toughened sPP. The effect was stronger in the injection molded composite exhibiting U 4.5 times higher than neat sPP, whereas in the compression molded composite, only 2.2-fold increase in U was achieved. It must be noted that AFM examination of the composite structure revealed the specific orientation of lamellae around chalk particles while SEM examination of impacted samples exhibited debonding of chalk particles from sPP matrix, which both are responsible for the toughening. Injection molding increased U even further; the flow during filling of a mold was beneficial for the toughness. X-ray examination evidenced orientation of the limit-disordered form I crystals in the injection molded bars with (200) crystallographic planes parallel to the flow direction, and the orientation was stronger in the composite than in neat sPP. Tensile testing of injection molded specimens showed that the presence of the filler did not worsen the drawability; the slight decrease of σ_y evidenced that the presence of chalk facilitated the plastic deformation of sPP matrix. Finally, it has to be noted that the cavitation at interfaces between the chalk and surrounding polymer, facilitating the plastic deformation of the latter, occurred during the impact test and also during uniaxial drawing of the composites. The (100) planes ((200) reflections are seen in WAXS patterns) are most densely packed in the limit-disordered form I sPP crystals and most probably (100) chain slips in those crystals are the easiest ones. The other slip systems may be activated between

less densely packed planes and they should be more difficult; in the orthorhombic unit cell, the distance between most densely packed (100) planes equals 1.43 nm while that between (010) planes is 0.56 nm. This implies a significant difference in critical resolved shear stresses between the easiest slip and the other that may be active in the limit-disordered form I sPP crystals, which is a prerequisite for the formation of the easy slip network and toughening.

ACKNOWLEDGMENTS

This research was supported by the Ministry of Science and High Education, Poland, Grant No. N507 592738, 2010–2013. The authors are indebted to Dr. T. Makowski for the AFM studies.

REFERENCES

1. Bartczak, Z.; Argon, A. S.; Cohen, R. E.; Weinberg, M. *Polymer* **1999**, *40*, 2347.
2. Y. Lin, C. M. Chan: In Advances in Polymer Nanocomposites: Types and Applications; Gao F., Ed.; Woodhead Publising: Cambridge, UK: **2012**; p 55–90.
3. Argon, A. S. The Physics of Deformation and Fracture of Polymers; Cambridge University Press: Cambridge, UK: **2013**.
4. Bartczak, Z.; Argon, A. S.; Cohen, R. E.; Kowalewski, T. *Polymer* **1999**, *40*, 2367.
5. Bartczak, Z.; Argon, A. S.; Cohen, R. E.; Weinberg, M. *Polymer* **1999**, *40*, 2331.
6. Muratoglu, O. K.; Argon, A. S.; Cohen, R. E.; Weinberg, M. *Polymer* **1995**, *36*, 921.
7. Muratoglu, O. K.; Argon, A. S.; Cohen, R. E. *Polymer* **1995**, *36*, 2143.
8. Schrauwen, B. A. G.; Govaert, L. E.; Peters, G. W. M.; Meijer, H. E. H. *Macromol. Symp.* **2002**, *185*, 89.
9. Corte, L.; Beaume, F.; Leibler, L. *Polymer* **2005**, *46*, 2748.
10. Corte, L.; Leibler, L. *Macromolecules* **2007**, *40*, 5606.
11. Hwang, W. R.; Peters, G. W. M.; Hulsen, M. A.; Meijer, H. E. H. *Macromolecules* **2006**, *39*, 8389.
12. Galeski, A.; Bartczak, Z. *Macromol. Symp.* **2003**, *194*, 47.
13. Bowden, P. B.; Young, R. J. *J. Mater. Sci.* **1974**, *9*, 2034.
14. Lin, L.; Argon, A. S. *Macromolecules* **1992**, *25*, 4011.
15. Zuiderduin, W. C. J.; Westzaan, C.; Huetink, J.; Gaymans, R. J. *Polymer* **2003**, *44*, 261.
16. Fu, S. Y.; Feng, X. Q.; Lauke, B.; Mai, Y. W. *Compos. B* **2008**, *39*, 933.
17. Guo, T.; Wang, L.; Zhang, A.; Cai, T. *J. Appl. Polym. Sci.* **2005**, *97*, 1154.
18. Levita, G.; Marchetti, A.; Lazzeri, A. *Polym. Compos.* **1989**, *10*, 39.
19. Rosa, C. D.; Auriemma, F.; Vinti, V. *Macromolecules* **1997**, *30*, 4137.
20. Rosa, C. D.; Auriemma, F. *Prog. Polym. Sci.* **2006**, *31*, 145.
21. Supaphol, P.; Harnisiri, W.; Junkasem, J. *J. Appl. Polym. Sci.* **2004**, *92*, 201.
22. Supaphol, P.; Harnsiri, W. *J. Appl. Polym. Sci.* **2006**, *100*, 4515.
23. Supaphol, P. *J. Appl. Polym. Sci.* **2001**, *82*, 1083.
24. Rodriguez-Arnold, J.; Zhang, A.; Cheng, S. Z. D.; Lovinger, A. J.; Hsieh, E. T.; Chu, P.; Johnson, T. W.; Honnel, K. G.; Geerts, R. G.; Palackal, S. J.; Hawley, G. R.; Welch, M. B. *Polymer* **1994**, *35*, 1884.
25. Tjong, S. C. *Mater. Sci. Eng. R Rep.* **2006**, *53*, 73.
26. Michler, G. H.; Batla-Calleja, F. J. Nano- and Micromechanics of Polymers. Structure Improvement and Modification of Properties; Hanser: Munchen, Cincinnati, **2012**; Chapter 10; p 369.
27. Jin, Y.; Rogunova, M.; Hiltner, A.; Baer, E.; Nowacki, R.; Galeski, A.; Piorkowska, E. *J. Polym. Sci. B Polym. Phys.* **2004**, *42*, 3380.
28. Bernal-Lara, T.; Masirek, R.; Hiltner, A.; Baer, E.; Piorkowska, E.; Galeski, A. *J. Appl. Polym. Sci.* **2006**, *99*, 597.
29. Langhe, D. S.; Hiltner, A.; Baer, E. *Polymer* **2011**, *52*, 5879.
30. Ma, Y.; Hu, W.; Reiter, G. *Macromolecules* **2006**, *39*, 5159.
31. Alexander, L. E. X-Ray Diffraction Methods in Polymer Science; Wiley-Interscience: New York: **1969**, p.70.
32. De Rosa, C.; Talarico, G.; Caporaso, L.; Auriemma, F.; Galimberti, M.; Fusco, O. *Macromolecules* **1998**, *31*, 9109.